Homopolymer Adsorption at the Liquid–Air Interface by XEWIF

Michael S. Kent,*,†,‡ Louis Bosio,§ and Francis Rondelez‡

Laboratoire de Physico-Chimie des Surfaces et Interfaces (associée au CNRS-URA 1379 et l'Université Paris VI), Institut Curie, Section de Physique et Chimie, 11 rue Pierre et Marie Curie, 75005 Paris, France, and Laboratoire Physique des Liquides et Electrochimie, ESPCI, 10 rue Vauquelin, 75005 Paris, France

Received March 5, 1992; Revised Manuscript Received July 16, 1992

ABSTRACT: The adsorption of poly(dimethylsiloxane) to the air surface from solution in bromoheptane (good solvent) and bromocyclohexane (T_Θ= 29 °C) has been studied by X-ray evanescent wave induced fluorescence (XEWIF). The sensitivity of the technique to the first ~40 Å of the surface region allows the determination of important qualitative features of the adsorbed concentration profiles. The effects of molecular weight, concentration, and solvent quality are examined in detail. In a good solvent, we find that the region of the profile nearest to the surface (~40 Å) is roughly independent of molecular weight in dilute solution, in agreement with theoretical predictions. Additional information about the adsorbed profile is obtained by varying the bulk polymer concentration. From these data we infer a profile with a high surface concentration (~90 ± 10%) which decays to under 20% within the first ~20 Å in the dilute and semidilute regimes. For near-Θ conditions, we find the adsorbed amount in dilute solution to be ~4 times larger than in a good solvent, with the profile decaying much more slowly with depth than in the good solvent. In addition, there appears to be a higher dependence on molecular weight for the region of the profile within ~40 Å of the surface. The results in good and near-Θ conditions are well described by both mean-field and scaling theories, while, on the contrary, the profile becomes qualitatively different in the proximity of the bulk coexistence curve (i.e., $T < T_c$).

I. Introduction

The study of adsorbed polymer layers has important applications in areas such as the stabilization of colloidal dispersions, lubrication, adhesion, and wetting. Much important work[1-3] has been done at the solid–liquid interface, but only a few studies[4-6] have been reported at the liquid–air interface. However, the latter interface offers definite advantages compared to the solid–liquid interface. First, most theories of polymer adsorption describe concentration profiles at equilibrium, which should be more readily attained at a fluid–fluid interface. Second, the liquid–air interface is easily accessed experimentally since a probing beam is not required to pass through a second condensed phase. Third, if one is careful to minimize vibrations, the liquid–air interface provides an extremely flat and reproducible surface. Fourth, there are no specific adsorption sites, and the substrate can therefore be treated as a continuum. Here we report a detailed study of the concentration profile of the neutral, flexible polymer poly(dimethylsiloxane) (PDMS) adsorbed from solution to the liquid–air interface under various thermodynamic conditions. The experimental probe is X-ray evanescent wave induced fluorescence (XEWIF). The small penetration depth (~40 Å) of the evanescent wave allows the determination of important qualitative features of the adsorbed concentration profiles. The surface tension of PDMS is lower than the surface tension of either solvent used in this study, and this difference provides the driving force for adsorption. Also important is the fact that PDMS is a liquid at ambient temperature and thus will more readily achieve equilibrium conformations than will glassy polymers. In this work we have explored the effects of molecular weight, bulk concentration, and solvent quality.

Theoretical approaches can be divided into mean-field[7,8] and scaling theories[9] depending upon whether correlations are taken into account. While the approaches are completely different, the two theories lead to very similar global features of the dilute-solution adsorbed profile, namely, an average thickness which in a good solvent varies with molecular weight (M) as $M^{0.4}$ (first moment of the scaling profile) or $M^{0.5}$ [approximate root-mean-square (RMS) thickness from the mean-field calculations of ref 8]. Moreover, very little variation of the adsorbed amount with bulk concentration is predicted over a large range from the dilute to semidilute regimes. There have been a number of attempts[3-5,10,11] to distinguish between the scaling law $\phi \sim z^{-4/3}$ for the monomer concentration profile predicted by scaling theory for good solvent conditions and the mean-field profile which does not follow a strict power law. However, it has proved difficult to make a clear distinction, with some groups[4,5,11] reporting $-4/3$ power law behavior and others observing no power law behavior at all.[3,10] The difficulty is likely due to the fact that in the scaling theory, power law behavior is only predicted for a certain central region of the profile, while, on the other hand, the mean-field profile will always appear to follow a power law over some limited range of depth. The extent of the power law region in the scaling theory ($D < z < R_g$, where D is a proximal length) and the magnitude of the deviation of the mean-field profile from a power law over a given range of z both depend on the parameter values used in the profile. In the present work, we do not place a strong emphasis on trying to distinguish between these two models but rather focus on qualitative, but yet important, features of the adsorption profiles.

II. Experimental Section

The PDMS samples used in this study are described in Table I. The first three are fractionated samples which were a generous gift from Alain Lapp (LLB, CEN Saclay). The fourth is a commercial sample obtained from Petrarch. The solvents 1-bromoheptane (BH) and bromocyclohexane (BC) were obtained from Aldrich and distilled under vacuum near room temperature just prior to use. BC is a Θ solvent for PDMS at 29 °C.[12] From turbidity measurements using an argon ion laser and a photomultiplier to measure the intensity of the transmitted beam, we have determined the critical temperature for the 140 K sample

† Permanent address: Division 1815, Sandia National Laboratories, Albuquerque, NM 87185.
‡ Institut Curie.
§ ESPCI.

0024-9297/92/2225-6231$03.00/0

Table I
Characteristics of the Poly(dimethylsiloxane) Samples

M_w	M_w/M_n	R_g (Å)[a] good solvent	R_g (Å)[a] θ solvent
2.5×10^4	3.9	60	45
1.4×10^5	1.3	170	110
1.15×10^6	1.2	600	290
1.1×10^5	7.5		

[a] Estimated from data for PDMS in toluene (good solvent)[26] and styrene (θ solvent at 35 °C).[27]

in BC to be 14.4 ± 0.3 °C. BH was determined to be a good solvent for PDMS at room temperature by the fact that no phase separation was observed for the unfractionated sample at 0 °C and over a range of concentrations. Estimates for the radii of gyration in the two solvents are also given in Table I. From this we calculate the overlap concentration ϕ^* delimiting the dilute and semidilute regimes to be $\phi^* = 0.011$ g/mL for the 140K sample in the good solvent BH, defining ϕ^* as $3M/4N_A\pi R_g^3$, which will be useful in the discussion to follow of the variation of the fluorescence intensity ratio with bulk concentration. Measurements were performed at room temperature (20–24 °C).

The strong adsorption of PDMS (surface tension $\gamma \sim 20$ dyn/cm) to the liquid–air interface from solution in BC ($\gamma \sim 34$ dyn/cm) has been described previously.[6,12] We have similarly established the strong adsorption of PDMS from solution in BH to the liquid–air interface by performing surface tension measurements based on the Wilhelmy hanging plate technique. A drop in surface tension from 27.7 dyn/cm for pure BH to 24.4 dyn/cm for a BH solution of low bulk concentration (0.002 g/mL) was observed and is consistent with previous measurements reported for PDMS in the good solvent toluene ($\gamma \sim 28$ dyn/cm).[13]

The XEWIF technique[6,14-16] is based on total external reflection which is achieved in this work by impinging an X-ray beam at grazing incidence onto a liquid surface from the air side. Below the critical angle (θ_c) for total external reflection, the X-ray beam penetrates into the solution as an evanescent wave, with the intensity falling exponentially to $1/e$ within ~40 Å from the surface for typical organic solvents. The evanescent wave is used to excite the fluorescence of the solvent. The fluorescence intensity corresponding to the bromine Kα and Kβ lines is measured as a function of incident angle (θ), and the ratio of the fluorescence intensity for the polymer solution to that of the pure solvent is taken at each angle to eliminate the need to determine geometrical factors such as the acceptance angle and efficiency of the detector, beam width, fluorescence yield, etc. If an adsorbed polymer layer is present at the surface, there will be a decrease in the fluorescence intensity for $\theta < \theta_c$ due to the depletion of bromine atoms in the region probed by the evanescent wave. For analysis of the experimental data, fluorescence intensity ratios were calculated from model profiles using a multiple-slab approximation of the interfacial profile, accounting for absorption in each slab and using the Fresnel coefficients to determine the reflected and transmitted beams at each interface.[6,16,17]

For the present system, the critical angles for the pure solvents are 1.26 mrad (BH) and 1.34 mrad (BC) and all other details can be found in ref 6. Compared with the original experimental procedure of Barton et al., the mechanical reproducibility of the angles has been improved such that no shifting of the data was required along the angular scale. The background intensity, coming principally from solvent molecules in the vapor phase, was determined by lowering the trough such that the beam passed cleanly just above the surface of the liquid and measuring the background fluorescence intensity. It was found to be 50 counts/20 s (BH) and 100 counts/20 s (BC) independent of polymer concentration, compared to a signal ranging from 25 000 to 200 counts/20 s (BH) and 300 counts/20 s (BC). The effective angular divergence was determined from the ratio of the fluorescence intensities from the pure solvents. Since the critical angles for BH and BC are slightly different, the fluorescence intensity ratio in the region of the critical angles deviates sharply from unity

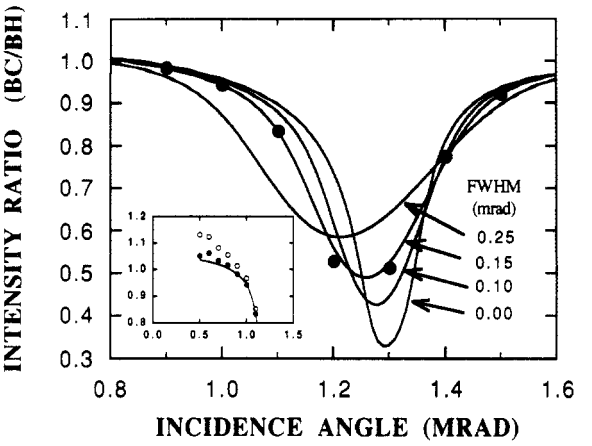

Figure 1. Determination of the effective beam divergence from the fluorescence intensity ratio for the pure solvents. The solid circles are the experimental values. The curves are calculated from the ratio of the fluorescence intensities at each angle (assuming Fresnel interfaces) convoluted with Gaussian functions of varying full width at half-maximum. The inset shows that the intensity ratio for the two solvents also serves to confirm the measurement of the background intensity. The open circles correspond to data with no background correction, while the solid circles correspond to the data after the background has been subtracted.

and the precise function is quite sensitive to the effective divergence. An example is given in Figure 1, which shows the ratio of the experimental fluorescence intensities for the two solvents (averaged over several angular scans). The curves are calculated from the ratio of the fluorescence intensities at each angle (assuming Fresnel interfaces) convoluted with Gaussian functions of varying full width at half-maximum (fwhm) to represent any effect which may lead to smearing of the angular resolution, such as the natural beam divergence or surface ripples. Note that the effective divergence is only important near the critical angle, where the penetration depth drops by several orders of magnitude. In Figure 1, the value of the fwhm which gives the best fit to the intensity ratio of the two solvents is 0.14 ± 0.05 mrad which agrees well with the natural divergence of the incident (0.13 mrad) and reflected beams (0.18 mrad at θ of 1.0 and 2.0 mrad) measured by scanning a narrow slit through the beams and measuring the intensity with a scintillation counter. However, such good agreement has not always been obtained, possibly due to slight shoulders in the incident beam which vary with the alignment of the instrument. The fluorescence intensity for θ near θ_c is likely to be very sensitive to such small effects, and so the measured effective beam divergence obtained from the intensity ratio for the two solvents was always used in the data analysis. The inset of Figure 1 shows that the fluorescence intensity ratio for two pure solvents also serves to confirm the measurement of the background intensity, which is important at the lowest angles. The open circles are the experimental data with no background intensity subtracted, while the filled circles are the experimental data after subtraction of the background intensity, which was determined in the manner described above. The good agreement of the filled circles with the calculated intensity ratio for the two pure solvents (solid curve) confirms this measure of the background intensity.

In the present work, the spatial resolution of the technique perpendicular to the surface is limited by several factors. First, the signal-to-noise is low (the intensity ratios deviate from unity by 20–40% with a standard deviation of ~5%). Second, while in principle it is possible to probe varying depths by varying the angle of incidence, this is difficult in practice. As shown in Figure 2 the penetration depth changes from ~40 Å to several thousand angstroms over a change in θ of only several tenths of a milliradian, whereas the effective angular divergence is 0.14 mrad. This makes it difficult to probe varying depths on the scale of the profile. Conclusions must thus be based on the data at low angles where the penetration depth is ~40 Å. Third, as will be shown below, the concentration profile in a good solvent decays much faster with depth than the intensity of the evanescent wave, even at the

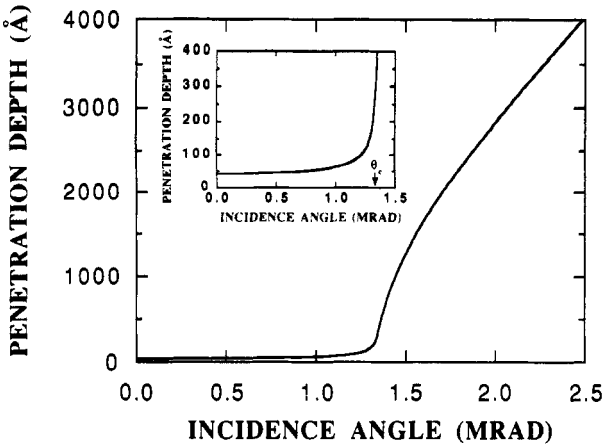

Figure 2. Penetration depth versus incidence angle for Mo K_α radiation incident on the free surface of pure bromocyclohexane.

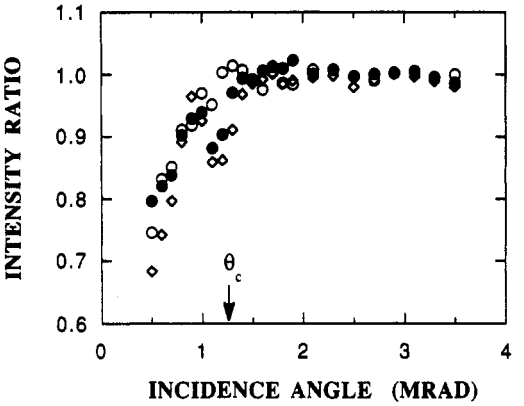

Figure 3. Fluorescence intensity ratio in the good solvent BH with $\phi_b = 2.0 \times 10^{-3}$ g/mL for PDMS molecular weights 2.5×10^4 (open circles), 1.4×10^5 (filled circles), 1.15×10^6 (open diamonds). These data reveal that the total monomer concentration within ~40 Å of the surface is roughly independent of the molecular weight.

lowest angles of incidence (i.e., smallest penetration depths). Determination of the precise form of the profile nearest the surface would require a minimum penetration depth even smaller than that in the present work. However, in the poorer solvent, the profile decays more slowly so somewhat more detail can be obtained.

III. Results

a. 1-Bromoheptane (Good Solvent). a.1. Molecular Weight Dependence. The fluorescence intensity ratio (fluorescence intensity for the polymer solution/fluorescence intensity for the pure solvent) versus incidence angle for the three fractionated PDMS samples in dilute solution (2.0×10^{-3} g/mL) in the good solvent BH is shown in Figure 3. Intensity ratios less than unity for $\theta < \theta_c$ prove the presence of an adsorbed polymer layer. The open symbols denoting the high and low molecular weights represent the average of three angular scans performed on a single solution for each sample. The dark symbols denoting the middle molecular weight represent results averaged for three separate solutions, where for each solution three angular scans were performed. Thus the data for the middle molecular weight are the most precise. Nevertheless, even for these data it was not possible to extract a unique profile. The profiles predicted by the mean-field and scaling models as well as a simple step profile are all consistent with these data over a range of parameter values (the ranges of acceptable parameter values for each profile will be described in the Discussion section). The dominant feature in Figure 3 is that there is little or no dependence on molecular weight.

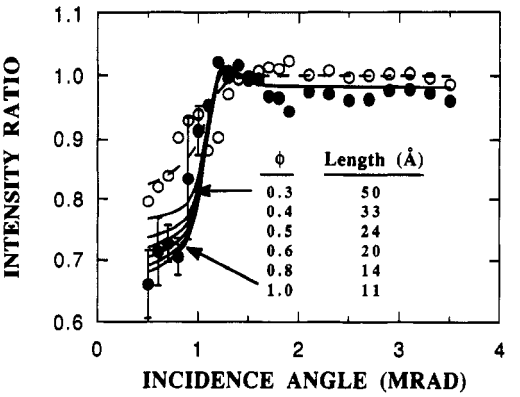

Figure 4. Variation of the fluorescence intensity ratio in the good solvent BH with bulk concentration: 140K sample with $\phi_b = 2.0 \times 10^{-3}$ g/mL (open circles); 110K sample with $\phi_b = 0.19$ g/mL (filled circles). From the decrease in the intensity ratio for $\theta < \theta_c$ with ϕ_b, limits can be determined for the parameters of model profiles. The dashed and solid curves were calculated using the step profiles given in Table II for $\phi_b = 2.0 \times 10^{-3}$ g/mL and $\phi_b = 0.19$ g/mL, respectively. The best fit is given by a step profile of roughly 80% and 14 Å, while step profiles with concentrations less than 50% are outside the error in the data (1 standard deviation). This represents a lower limit for ϕ_s for any monotonically decreasing profile.

a.2. Concentration Dependence. The bulk concentration ϕ_b has been varied from 2.0×10^{-3} to 0.19 g/mL in BH (which covers from the dilute well into the semidilute regime for PDMS of molecular weights 110K and 140K). The variation of the intensity ratio is shown in Figure 4. Three features are observed in the data as a function of bulk concentration. First, the intensity ratios at large incidence angles are not strictly unity, which may appear surprising. The few percent decrease is due to the near but not complete compensation of two effects. The X-ray absorptivity of the bulk solution is only approximately proportional to the bromine concentration, while the fluorescence signal is precisely proportional to the bromine concentration. Thus, for a 20% PDMS solution, the beam penetrates slightly less than 20% further into the bulk than for the pure solvent (not precisely 20% further because PDMS contributes slightly to the absorptivity), while the fluorescence yield at a particular depth is proportional to the bromine concentration which has decreased precisely 20%. The second feature is the small bump near the critical angle for the 20% solution. This occurs because the critical angle is slightly lower for this solution than for the pure solvent, as the real part of the X-ray refractive index for PDMS (7.24×10^{-7}) is slightly lower than that for the solvent (7.96×10^{-7}). On the contrary, no bump occurs for the dilute solution because in that case the critical angle is essentially the same as that for the pure solvent.

The third and most important feature for this study is that for $\theta < \theta_c$ the intensity ratios are much lower for the more concentrated solution. It is important to note that this does not require increased polymer absorption with increasing bulk concentration but will also result from an adsorbed profile which is independent of bulk concentration if the profile decays with depth faster than the evanescent wave. This is illustrated in Figure 5 for the extreme case of a step profile. The solid lines represent a step profile with a polymer volume fraction of 1.0 and a length of 11 Å, which is consistent with the dilute-solution data in Figure 4. The shaded region represents the additional polymer present in the concentrated solution with respect to the dilute solution ($\phi_b \to 0$). The decrease in the intensity ratio over this increase in bulk polymer concentration is determined by the convolution of the

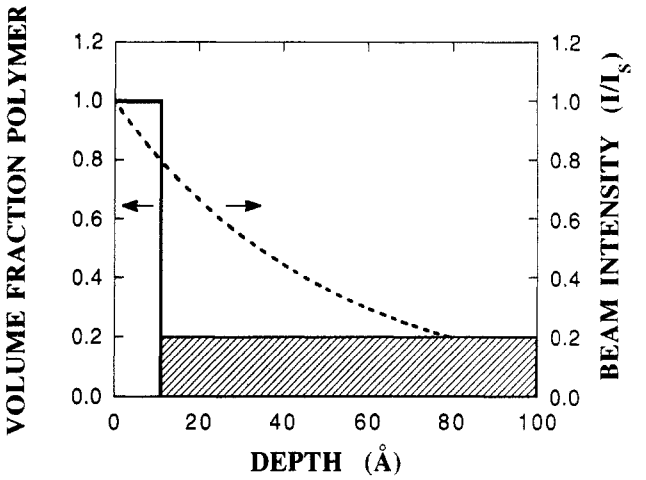

Figure 5. Interpretation of the variation of the fluorescence intensity ratio with bulk concentration in the good solvent BH. The intensity profile of the evanescent wave (dotted curve) at $\theta = 0.5$ mrad (normalized to the intensity at the surface) is shown along with the polymer concentration profile for $\phi_b \to 0$ and $\phi_b = 20\%$, assuming an adsorbed step profile of 11 Å and $\phi = 1.0$ which is independent of ϕ_b. The shaded region represents the additional polymer present in the 20% solution. The decrease in the intensity ratio at $\theta = 0.5$ mrad is given by the convolution of the shaded region with the intensity of the evanescent wave.

shaded region with the intensity of the evanescent wave (given by the dotted curve for $\theta = 0.5$ mrad). Once again, more polymer means less solvent and, therefore, a lower bromine concentration. Since the beam intensity profile decreases exponentially with depth, a greater decrease in the fluorescence intensity ratio with ϕ_b results if the shaded area extends closer to the surface (numerical examples will be given in the Discussion section). This can actually be used to great advantage, as it enables some details of the profile to be obtained on length scales smaller than the penetration depth of the evanescent wave. Of course, any increase in adsorption with bulk concentration will also contribute to the decrease in the intensity ratio, but we expect this to be of secondary importance since the experimental concentration range is believed to be within the adsorption plateau regime.

b. Bromocyclohexane (T_Θ = 29 °C). b.1. Comparison with Good Solvent. A comparison of the fluorescence intensity ratios for the 140K sample at a dilute bulk concentration of 2.0×10^{-3} g/mL in BH (good solvent) and BC (near-Θ solvent) is shown in Figure 6. Each curve represents results averaged for three separate solutions where for each solution three angular scans were performed. The lower values of the intensity ratio at $\theta < \theta_c$ in BC indicate a much greater adsorbed amount in the first ~40 Å than in BH. In addition, for the data in BC we observe a slight, however significant, rise in the intensity ratio with decreasing incidence angle as the critical angle is approached from high angles. This feature results from the fact that the X-ray adsorptivities of the polymer and solvent differ significantly (the adsorptivity is not important for $\theta < \theta_c$, but becomes important for $\theta \geq \theta_c$ where the beam penetrates into the solution over longer distances). The effect is not simply a function of the amount of adsorbed polymer but is also a strong function of the extension of the profile from the surface. For example, virtually no rise would be observed for a 40-Å melt of polymer at the surface, whereas a 200-Å layer of 20% (thus with the same adsorbed amount) would produce a substantial rise. No effect results unless a significant concentration of polymer is present at distances ~80 Å or more from the surface. Thus, the rise in the intensity

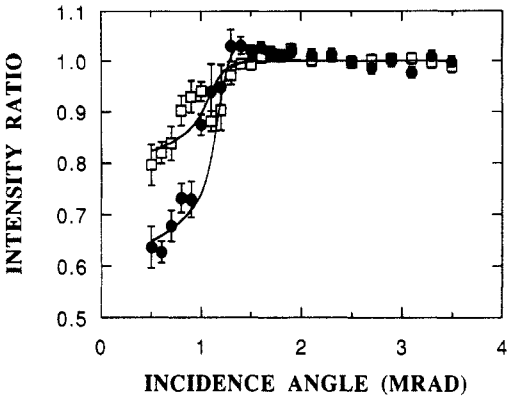

Figure 6. Fluorescence intensity ratio for the PDMS 140K sample with $\phi_b = 2.0 \times 10^{-3}$ g/mL in the good solvent BH (open squares) and the near θ solvent BC (filled circles). The error bars represent 1 standard deviation. The solid curves were calculated using the profiles shown in Figure 7 (discussed in the text). The lower values of the intensity ratio for $\theta < \theta_c$ in BC indicate a much greater adsorbed amount, while the slight rise in the intensity ratio near θ_c in BC indicates that the profile extends much further from the surface than in BH.

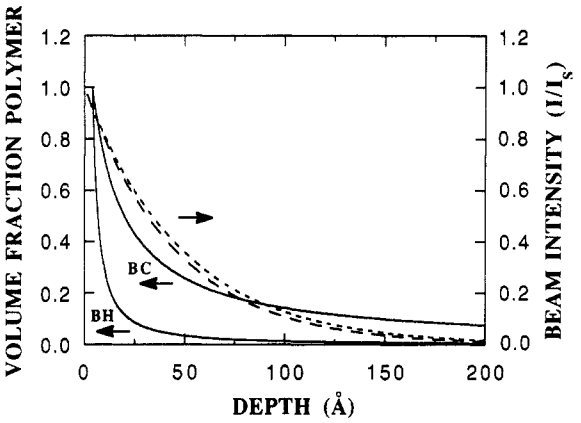

Figure 7. Comparison of the intensity profile of the evanescent wave in BH (dashed curve, short dashes) and BC (dashed curve, long dashes) at $\theta = 0.5$ mrad (normalized to the intensity at the surface) with polymer concentration profiles which are consistent with the data in Figure 6. The profiles were calculated from eq 1 with $a = 4$ Å, $D = 0$ Å, and $\phi_s = 1$ (BH) and $a = 4$ Å, $D = 12$ Å, and $\phi_s = 1$ (BC). Since the profile in BC decays much more slowly than in BH, the fluorescence intensity ratio at $\theta < \theta_c$ will be much less sensitive to variations in ϕ_b.

ratio near θ_c in BC implies that the concentration profile extends much further from the surface in BC than in BH.

b.2. Concentration Dependence. The effect of the bulk concentration has also been examined in BC. From the earlier discussion regarding the decrease in the intensity ratio at $\theta < \theta_c$ observed with an increase in bulk concentration in BH, one expects the same effect to be smaller in BC since the dilute-solution profile decays from the surface much more slowly. This is illustrated in Figure 7, which shows the dilute-solution profiles used for the calculated curves in Figure 6 (the origin of these profiles will be described below in the Discussion section) along with beam intensity profiles for $\theta = 0.5$ mrad in the two solvents. If ϕ_b is increased from dilute to 20% in the good solvent BH (and assuming an adsorbed profile which is independent of ϕ_b), the depth at which the profile decays to ϕ_b is around $z \sim 15$ Å, where the intensity of the evanescent wave is still large. By contrast, in the near-Θ solvent BC, for the same increase in ϕ_b the profile is cut off at ~70 Å, where the intensity of the evanescent wave is small. Thus, in BC, the level of the bulk concentration is not expected to influence the fluorescence intensity at $\theta < \theta_c$ until $\phi_b > \sim 40\%$. Little or no variation was indeed

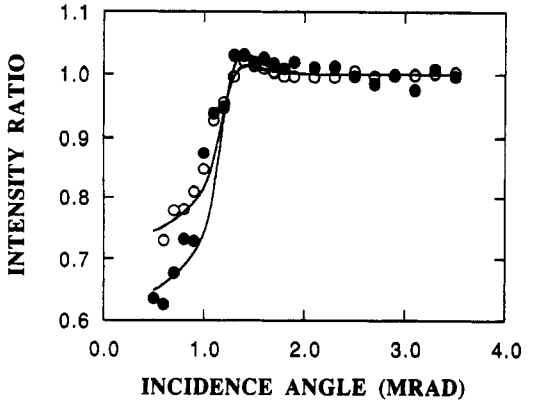

Figure 8. Fluorescence intensity ratio in BC with $\phi_b = 2.0 \times 10^{-3}$ g/mL for PDMS molecular weights 2.5×10^4 (open circles) and 1.4×10^5 (filled circles). The temperature of the measurement (20–24 °C) was below T_θ (29 °C) but well above T_c for the two lower molecular weights (T_c = 14.4 °C for the 140K sample). Thus the solvent condition is characterized as near-Θ. A greater variation with molecular weight is observed in BC than was observed in BH.

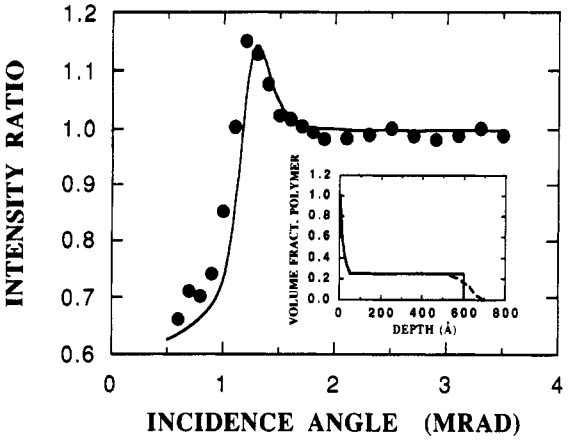

Figure 9. Fluorescence intensity ratio in BC with $\phi_b = 1.3 \times 10^{-4}$ g/mL for the 1150K sample. Here the measurement temperature was below T_c, and the solvent condition is characterized as poor. The large maximum near θ_c implies a profile qualitatively different than that for the two lower molecular weights of Figure 8. The solid line corresponds to the curve calculated using the profile in the inset (see text).

observed in BC for the range of bulk concentrations from 0.002 to 0.05 g/mL. This observation also supports the assumption that there is little or no increase in the adsorbed amount with bulk concentration over this range.

b.3. Molecular Weight Dependence. The variation with molecular weight in BC is shown in Figures 8 and 9. For the two lower molecular weights (Figure 8) the concentration was 2.0×10^{-3} g/mL. While the temperature of the measurement (20–24 °C) was below T_θ (29 °C), it was still well above T_c for the two lower molecular weights (T_c = 14.4 °C for the 140K sample) and so we characterize the thermodynamic condition for these solutions as near-Θ. The important feature in these data is that the intensity ratios for $\theta < \theta_c$ are lower for the 140K sample than for the 25K sample. For the highest molecular weight (Figure 9) the solvent condition is considered to be poor, as the temperature of the measurement was below the critical temperature (T_c). In this case, a lower concentration (1.3×10^{-4} g/mL) was used to avoid phase separation in the bulk. These data show a much larger maximum near the critical angle than for the two lower molecular weights. For this molecular weight, it was also observed that the fluorescence intensity in the region of the critical angle varied with time during the first few hours, finally leveling off at the values shown, while no variation with time was observed with the other molecular weights over ~24 h.

IV. Discussion

a. 1-Bromoheptane (Good Solvent). a.1. Molecular Weight Dependence. The dominant feature in Figure 3 is that there is little or no dependence on molecular weight. This is entirely consistent with both scaling and mean-field theories which predict the portion of the profile near the surface to be independent of molecular weight, while the tail of the distribution is expected to vary considerably with molecular weight. Since for $\theta < 0.8\theta_c$ the experiment probes the first ~40 Å from the surface, i.e., distances much smaller than the estimated radii of gyration (R_g) of the polymers in this work (Table I), these XEWIF data are not sensitive to the tail of the distribution. Information about the tail of the distribution should be contained in the data for θ between $0.8\theta_c$ and θ_c; however, any small effect which may exist in that angular range is entirely lost in the scatter in the data.

While the data in Figure 3 show no dependence on molecular weight, there are a range of parameter values

Table II
Step Profiles Which Are Consistent with the Dilute-Solution Data of Figures 3 and 4

length (Å)	vol %	length (Å)	vol %
11	100	24	50
14	80	33	40
20	60	50	30

for even a simple step profile which are consistent with these data. However, the range of parameters can be further constrained by comparison with data for different bulk concentrations, as discussed below in section IV.a.2. Table II gives a family of step functions, all of which are consistent with the experimental intensity ratios for the dilute-solution data in Figure 3. It will be shown in section IV.a.2 that in order to be consistent with the variation with bulk concentration, ϕ_s must be greater than 50%. For the step profiles in Table II with concentrations greater than 50%, the total monomer concentration in the first 40 Å is roughly the same. This also holds for scaling and mean-field profiles for the range of parameters which are consistent with the variation with bulk concentration. Thus, the essential conclusion from the data in Figure 3 is that the total monomer concentration in the first 40 Å is roughly independent of molecular weight. There may be a small variation (<~20%) which would not be observable with the present technique. We note that in a recent report of neutron reflectivity for PDMS adsorbed to the air surface from toluene,[5] the molecular weight independence of the first ~30 Å of the profile was an important assumption used in the data analysis. This hypothesis is supported by the present data.

It should be noted that this result is not inconsistent with the larger dependences on molecular weight for the thickness of adsorbed layers (typically the average thickness goes as $M^{0.4-0.6}$) which have been reported with other techniques.[1,3-5,18,19] The difference arises because the present technique is mostly sensitive to the first ~40 Å, whereas the techniques reporting higher molecular weight dependences have more sensitivity to larger depths and thus to the tail of the distribution. Ellipsometry[18] and optical evanescent wave induced fluorescence[19] have been shown to measure the zeroth and first moments of the distribution. As mentioned above, the first moment of the scaling profile scales with $M^{0.4}$. Some sensitivity to the tail of the distribution is also expected with SANS and X-ray and neutron reflectivity.[3-5,10,11] Thus the

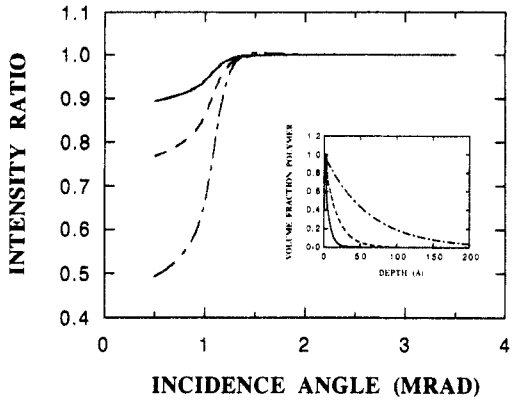

Figure 10. Predicted variation in the fluorescence intensity ratio in BH over the present range of molecular weights for an exponential profile with decay length proportional to R_g. The profiles are given in the inset. The lack of a variation in the experimental fluorescence intensity ratio with molecular weight in Figure 3 thus implies that any variation of the profile with molecular weight must occur mainly in the tail of the profile.

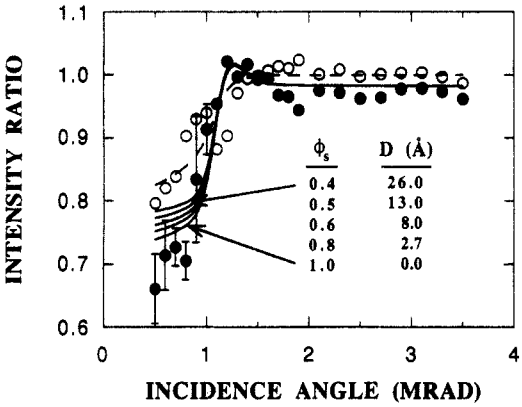

Figure 11. Calculated variation of the fluorescence intensity ratio with bulk concentration in the good solvent BH using eq 1 (scaling) with the monomer length fixed at 4 Å. Open and filled circles have the same significance as in Figure 4.

molecular weight independence of the data in Figure 3 apparently results because the profile varies with molecular weight only in the tail, at depths where XEWIF is not sensitive. By contrast, if the entire profile scaled with the radius of gyration rather than only the tail of the distribution, a significant variation would have been observed in the data in Figure 3. This is illustrated in Figure 10 for an exponential polymer volume fraction profile whose e-fold decay length varies as R_g or $M^{0.6}$ over the present range of M.

a.2. Concentration Dependence. The measurement of the intensity ratio for two bulk concentrations (in this case, 0.002 and 0.19 g/mL) provides two constraints for any set of model parameters and thus limits the ranges of possible values. In particular, a unique best fit can then be determined for a two-parameter step profile. On the other hand, a unique best fit cannot be obtained for scaling and mean-field profiles involving three parameters, so ranges for two parameters will be determined for given values of the third parameter.

a.2.1. Step Profile. The dotted and solid lines in Figure 4 show the calculated fluorescence intensity ratios using the step profiles of Table II and the experimental bulk concentrations of 0.002 g/mL (dotted line) and 0.19 g/mL (solid lines). The dotted line actually represents the calculated fluorescence intensity ratios for all the step profiles in Table II in dilute solution, which all give virtually the same curve. However, there is a large variation for the same series of profiles in the 20% solution. Here we have neglected any small increase of adsorption which may occur with bulk concentration. In Figure 4 the best fit to the data for both bulk concentrations is given by a step of roughly 80% and 14 Å, while step profiles with concentrations less than 50% are outside the error in the data (1 standard deviation). This value actually represents a lower limit for the surface concentration ϕ_s for any monotonically decreasing profile. Profiles which are smoother than a step function will extend further from the surface when constrained to fit the dilute-solution data than will the step profile, if ϕ_s of the smooth profile is equal to ϕ of the step profile. Recalling the discussion of Figure 5, this means that a step profile will give the greatest variation in the fluorescence intensity ratio with bulk concentration and thus implies that 50% is a lower limit for ϕ_s for any monotonically decreasing profile.

a.2.2. Scaling Profile. In Figure 11 we compare the data of Figure 4 with the following three-parameter (ϕ_s,D,a) scaling profile:

$$\phi(z) = \phi_s \quad \text{for } 0 < z \le a$$

$$\phi(z) = \phi_s(a + \mu D)/(z + \mu D)^{\mu} \quad \text{for } a < z \le L$$

$$\phi(z) = \phi_b \quad \text{for } z > L \qquad (1)$$

where a is a monomer length, z is the depth measured from the surface, and L is a cutoff length. The parameter μ takes the values $^4/_3$ and 1 in good and Θ solvents, respectively. In dilute solution, we set L at $2R_g$, whereas in semidilute solution L is the depth at which $\phi(L) = \phi_b$. In semidilute solution, L is expected to be roughly equal to the correlation length $\xi = R_g(\phi^*/\phi_b)^{3/4}$. In eq 1, the proximal length defined by $|(1/\phi)(d\phi/dz)|^{-1}_{z=a}$ is given by $(a + \mu D)/\mu$. Thus in eq 1 the monomer length a and the initial slope at $z = a$ are allowed to vary independently. This profile is valid for the range of ϕ_b corresponding to the plateau in the adsorption isotherm. Since the scaling theory leading to eq 1 does not attempt to treat in detail the region near the cutoff L, this profile neglects any small changes in adsorbed amount which may occur with bulk concentration. It has been estimated that the end of the adsorption plateau is reached when ξ becomes equal to the proximal length.[20] We estimate ξ in the more concentrated solution to be ~20 Å while below we find a proximal length of ~4 Å, so we expect that eq 1 still holds for the concentrated solution. In this regime, changes in ϕ_b affect only L, while the profile near the surface is unchanged.

Figure 11 compares the experimental data with calculated curves using eq 1 where ϕ_s and D are varied for a = 4 Å (the value of the monomer length which allows the closest agreement with both sets of data). We find that the scaling profile is not able to reproduce the variation with bulk concentration that is observed experimentally. The comparison is performed by first determining a set of parameters which gives good agreement with the dilute-solution results and then using the same parameters to calculate the results for the concentrated solution.[21] The best fit ($\phi_s = 1.0$, $D = 0$ Å, $a = 4$ Å) falls outside 1 standard deviation of the experimental data but within 2 standard deviations. We note that the above set of parameters agrees well with the profile recently determined by neutron reflectivity for PDMS adsorbed at the air surface from dilute solution in toluene,[5] where $\phi_b = 0.96$, $D = 0.075$ Å, and $a = 5.2$ Å were reported (the same profile was used; however, their notation is somewhat different). The low

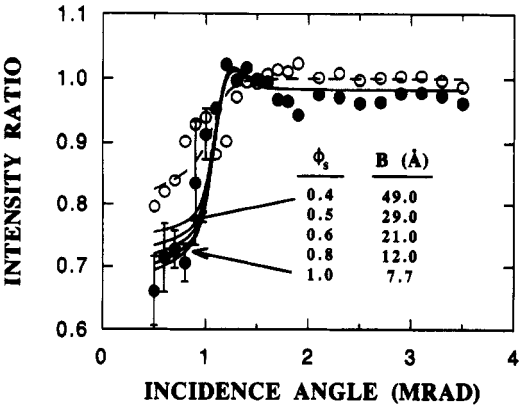

Figure 12. Calculated variation of the fluorescence intensity ratio with bulk concentration in the good solvent BH using eq 2 (mean-field) with the monomer length fixed at 5 Å. Open and filled circles have the same significance as in Figure 4.

values of D indicate that the proximal length corresponds roughly to the value of a.

a.2.3. Mean-Field Profile. The three-parameter (ϕ_s, B, a) mean-field profiles were calculated as[13,22]

$$\phi(z) = \phi_s \quad \text{for } 0 < z \le a$$

$$\phi(z) = \phi_b \coth^2((z-a)/\xi_E - \sigma) \quad \text{for } a < z \le L \quad (2)$$

where $\xi_E = B/\phi_b^{0.5}$ is the Edwards correlation length and σ is a dimensionless constant determined from the value of ϕ_s. We note that in eq 2, in contrast to eq 1, there is a small dependence of the adsorbed amount on ϕ_b. The approximate analytical form in eq 2 is valid over a range of dilute–semidilute concentrations in which the monomer–monomer interactions are dominated by the two-body term. For very dilute solutions, the translational entropy term in the free energy must be included. However, this term is expected to be small for $\phi_b > 1/N$ (where N is the number of monomers per chain), which is true here. Similarly, at high concentrations, higher order terms in the concentration dependence must be included. However, eq 2 is believed to be a good approximation to the exact mean-field profile over the present range of bulk concentrations, as eq 2 has been found to be in reasonable agreement with the numerical SCF calculations of Scheutjens and Fleer over this range.

The constant B is given by $a/(3\nu)^{0.5}$, where νa^3 is the dimensionless excluded-volume parameter. The exact value of ν is not known for PDMS in bromoheptane, but the value of 0.16 reported[13] for PDMS in toluene may serve as a rough estimate. A reasonable range of B values is then from 4 to 13 Å, using monomer lengths ranging from 3 to 7 Å and ν ranging from 0.10 to 0.20. By comparing the experimental data with eq 2, limits for the ranges of ϕ_s and B can be determined for a given value of a.

Figure 12 compares mean-field profiles for fixed a (5 Å) and varying ϕ_s and B with the experimental data of Figure 4. Again, each set of parameters gives good agreement with the dilute-solution data, and conclusions are based on the ability of the same set of parameters to reproduce the variation of the intensity ratio with bulk concentration. Good agreement with both sets of data is obtained for ϕ_s ranging from 0.8 to 1.0, with corresponding B values of 8–12 Å, which are within the estimated range given above. Values of ϕ_s less than 0.8 lead to poorer agreement with the data from the 20% solution and also require values of B to fit the dilute-solution data which are larger than the estimated range given above. Similar conclusions are obtained if the monomer length is varied within reasonable limits. This is shown in Table III, in which sets of parameters ϕ_s and B are given for a = 3, 5, and 7 Å, where each set gives good agreement with the dilute-solution data. From among these, the sets of parameters which give good agreement to the concentrated solution data are indicated by asterisks. We find that the acceptable range for ϕ_s is from 0.8 to 1.0 in each case.

The main result from the comparison of model profiles with the data in Figure 4 is that the concentration must be high at the surface (90 ± 10%) and decay to under 20% within the first ~20 Å. This conclusion is consistent with recent neutron reflectivity results for the adsorption of PDMS at the air surface of toluene.[5] Regarding the comparison between mean-field and scaling theories, we find that the mean-field theory is better able to reproduce the variation with bulk concentration. However, the lack of precise agreement with the scaling profile is probably due to the abrupt cutoff at $z = L$, which neglects any small dependence of the adsorbed amount on concentration and which was never treated in detail in the theory. We note that in the dilute-solution neutron reflectivity work of ref 5, the mean-field profile was ruled out because a power law of −2 for the dependence of $\phi(z)$ on z was found to be inconsistent with the reflectivity data. It is our view that the mean-field profile cannot be ruled out on the basis of the inadequacy of a −2.0 power law. The mean-field profile above (as well as profiles from the numerical self-consistent mean-field calculations of Scheutjens and Fleer) can be approximated as a power law only for a very limited range of depth. If a power law is forced through the mean-field profiles given in Table III over the range of z from 10 to 100 Å, we find a range of exponents from 1.4 to 1.9 for the sets of parameters which correspond to reasonable B values (see Table III). An exponent of 1.5 was reported in ref 5 to be within experimental error. We thus believe that comparison must be made with the precise form of the mean-field profile before it can be judged to be inadequate.

Finally, we note that ϕ_s observed in both studies of PDMS adsorbed at the air surface of a good solvent (the present work and ref 5) is much higher than that observed for other polymers adsorbed at the solid–liquid interface,[1,3] where typical values fall in the range 0.2–0.6. This may be due to the extreme flexibility of PDMS, the fact that PDMS is a liquid at room temperature (the other systems involved polymers which are glassy at room temperature), and additional mobility which may be possible at a fluid–fluid interface.

b. Bromocyclohexane (T_Θ = 29 °C). b.1. Comparison with Good Solvent. Figure 13 shows a comparison of the results in BC from Figure 6 with calculated curves using mean-field, scaling (for the Θ-solvent case), and step profiles. The surface concentration is expected to be as high or higher in the poorer solvent BC than in BH since the osmotic repulsion between monomers is greatly reduced. Thus we consider only profiles with $\phi_s \ge 0.80$. One sees immediately that step functions with $\phi_s \ge 0.80$ are not consistent with these results. The step profile which gives the best fit to the data has a length of 130 Å and ϕ = 0.45. We consider such a low value of ϕ unacceptable considering the range of ϕ_s obtained in the good solvent BH. On the contrary, the mean-field and scaling profiles both give good agreement with the data over a realistic range of parameters. The inset shows the profiles used to calculate the curves in Figure 13. Indeed, we find very little difference between the scaling and mean-field profiles.

In the mean-field profile in eq 2, the dependence on solvent quality is included explicitly in the value of the

Table III
Sets of Parameters for the Mean-Field Profile (Equation 2) Which Are Consistent with the Dilute-Solution Data of Figures 3 and 4[a]

a = 3 Å			a = 5 Å			a = 7 Å		
ϕ_s	B	x^b	ϕ_s	B	x^b	ϕ_s	B	x^b
1.0*	11.0	−1.57	1.0*	7.7	−1.75	1.0*	4.7	−1.94
0.8*	15.5	−1.39	0.8*	12.0	−1.56	0.8*	9.0	−1.79
0.6	24.0	−1.12	0.6	21.0	−1.22	0.6	17.5	−1.36
0.5	34.0		0.5	29.0		0.5	26.0	
0.4	55.0		0.4	49.0		0.4	45.0	

[a] ϕ_s is the volume fraction of polymer at the surface (z = 0), a is a monomer length, and B (in Å) is related to the Edwards correlation length ξ_E by $\xi_E = B/\phi_{bulk}^{-0.5}$. Asterisks indicate the sets of parameters which give the best agreement with both sets of experimental data in Figure 4. [b] x represents the exponent if the profile is approximated by a power law (least-squares fit) over the range of z from 10 to 100 Å.

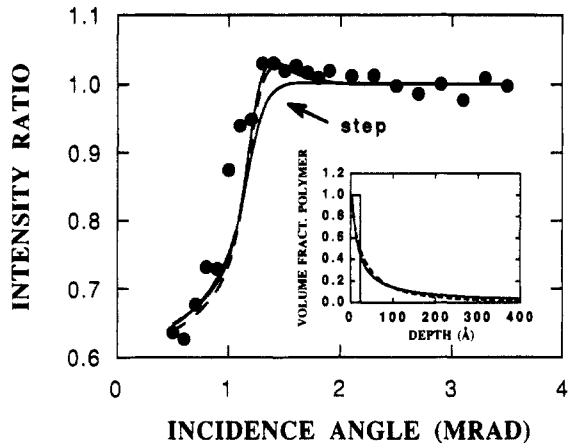

Figure 13. Fluorescence intensity ratio for the PDMS 140K sample with $\phi_b = 2.0 \times 10^{-3}$ g/mL in the near-Θ solvent BC (filled circles) compared to calculated curves using step (ϕ = 1.0, length = 32 Å), scaling (a = 4 Å, D = 12 Å, ϕ_s = 1), and mean-field (a = 4 Å, B = 50 Å, ϕ_s = 1) (dashed line) profiles shown in the inset. Step profiles are not consistent with the experimental data.

excluded-volume parameter ν. Larger values of B are expected as the value of ν (and, thus, the quality of the solvent) decreases. However, this equation is only valid when the term involving two-body interactions dominates the solution free energy density. It is therefore not rigorously valid near the Θ temperature when the two-body term becomes small or for $T < T_\Theta$ where ν is negative.[12,23] However, since no analytical expression exists for the Θ-solvent case, we have nevertheless used eq 2 as an approximate form. At this stage we would like to point out what we believe to be an error in ref 6 in the equation for the mean-field profile. There, R_g appears in place of the correlation length ξ_E, and this leads to incorrect dependences of the profile on molecular weight and solvent quality. In ref 6, the mean-field profile was rejected on the grounds that the correlation length determined from least-squares fits was much larger than estimates of R_g. We note that large values of ξ_E are indeed expected for small values of ν and for dilute solutions.

While it is not possible to extract unique values for the three parameters in each profile, choosing the reasonable values ϕ_s = 1.0 and a = 4 Å, one obtains D = 12 Å (scaling) and B = 50 Å (mean-field). This value of D is much larger than that obtained in the good solvent BH. Thus, we find that the variation in the value of μ from $^4/_3$ to 1 in eq 1 alone is insufficient to describe the difference in the profiles in good and Θ solvents. Either a or D must vary also.

The adsorbed amount (5–6 mg/m^2), estimated from the integral (cutoff at $2R_g$) of mean-field and scaling profiles in the inset of Figure 13, is roughly 4 times as large as that in BH (1.4 mg/m^2). This increased adsorption in a poorer solvent is indeed expected, as the adsorption process is a competition between the attraction to the surface ($\Delta\gamma$) and the cost in free energy to distort the chain conformations and form a layer of elevated polymer concentration. The effective repulsion between monomers is lower in a poorer solvent; thus, one expects a surface to be able to support a larger adsorbed amount in a poorer solvent than in a good solvent, other factors being equal. This has been demonstrated by numerical solutions to the mean-field equations[8] and has been observed in ellipsometric measurements for the adsorption of polystyrene at the chrome–organic solvent interface, where adsorbances of ~1 and ~0.65 mg/m^2 were reported in the good solvents carbon tetrachloride and toluene while ~5 mg/m^2 was observed in the Θ solvent cyclohexane.[18]

Before assigning the effect in Figure 6 solely to the difference in solvent quality, however, it must be noted that the surface tensions of the two solvents also differ. The surface tension of BC is roughly 14 dyn/cm higher than that of PDMS at room temperature, whereas the difference is roughly 8 dyn/cm in BH. The additional 6 dyn/cm difference could possibly contribute to the increased adsorption in BC. However, the magnitude of the difference in surface tension becomes unimportant when the concentration of polymer at the surface approaches unity, and since the results in BH imply that ϕ_s is already very high, we believe that the increased adsorption in BC is due mostly to the difference in solvent quality.

Regarding the molecular weight dependence in BC shown in Figure 8, one observes that for $\theta < \theta_c$ the fluorescence intensity ratio for the middle molecular weight is clearly lower than that for the lower molecular weight. This suggests that there is a greater variation of the profile in the first ~40 Å with molecular weight in the poorer solvent BC than in BH (compare with the data in Figure 3). However, the percentage increase in adsorbed amount in the first ~40 Å with molecular weight that we observe from the data in Figure 8 is somewhat larger than the percentage increase predicted by mean-field theory for the total adsorbed amount (integrating the adsorbed profile to $z = \infty$). The SCF calculations of Scheutjens and Fleer[8] predict a ~35% increase in the total adsorbed amount for the range of molecular weights corresponding to the low and middle molecular weights in Figure 8, whereas we estimate an increase in the adsorbed amount in the first ~40 Å of roughly 80 ± 40%. A thorough comparison with the calculations of ref 8 requires information about the variation in the tail of the distribution as well as the region nearest the surface, which cannot be obtained with this technique at present. We note that the greater increase with molecular weight observed here may be due to the fact that the solvent condition is slightly less than Θ here (the dependence on molecular weight increases with decreasing solvent quality[8]).

b.2. Poor Solvent. While the three molecular weight PDMS samples were studied at the same temperature in

BC, the solvent condition was much different for the highest molecular weight than for the other two, as the measurement temperature was below T_c for that sample. We find that the data for the highest molecular weight in Figure 9 are much different than those of the two lower molecular weights in Figure 8 and cannot be fitted by the mean-field and scaling profiles in eqs 1 and 2 or by a single step profile when $\phi_s > 0.8$. The large maximum in the data near the critical angle demands a much larger adsorbed amount than for the other two molecular weights.

A rigorous numerical mean-field analysis[23] (as opposed to the approximate form given by eq 2) has predicted the development of a plateau region in the profile as the coexistence curve is approached, where the plateau concentration is equal to that of the concentrated branch of the coexistence curve. We have found that the present data are quite consistent with this picture, although the value for the concentration corresponding to the concentrated branch of the coexistence curve at the temperature of the measurement is not precisely known. The solid curve in Figure 9 corresponds to the calculated fluorescence intensity ratio using the same profile as in Figure 13 for the 140K sample but with a plateau region of volume fraction 0.25 extending to $z = 600$ Å (shown in the inset to Figure 9). For this rather crude model profile, we find that there are definite limits for the values of the length and concentration of the plateau which give good agreement with the experimental data. The maximum near the critical angle cannot be reproduced for plateau concentrations lower than ~20%, while the ratios at the lowest angles are much lower than the experimental data for plateau concentrations greater than 30%. Within this range of plateau concentrations, the maximum near the critical angle cannot be reproduced for plateau lengths less than ~400 Å. However, the intensity ratios are insensitive to changes in the length of the plateau region beyond ~800 Å.

In the Results section, we mentioned that the fluorescence intensity ratios for this sample varied with time during the first few hours, in contrast to the data for the two lower molecular weight samples. In particular, after the first scan the bump in the intensity ratio near θ_c was not present, while the values for $\theta < \theta_c$ were nearly the same as in Figure 9. The bump then appeared and grew with time during several hours. Our hypothesis is that there is a dense adsorbed layer of the type predicted by mean-field and scaling theories near the Θ point which forms very rapidly, whereas the second (less dense) layer is brought about by the proximity to the coexistence curve and forms more slowly. Johnson et al.[24] have recently reported increased polymer adsorption as the coexistence curve is approached for the system polystyrene/cyclohexane/oxidized silicon. Further work on this subject is underway in our laboratory and will be reported elsewhere.[25]

V. Conclusion

XEWIF has been used to examine the variation in the concentration profile of PDMS adsorbed at the liquid–air interface with molecular weight, bulk concentration, and solvent quality. In the good solvent BH, the fact that no variation with molecular weight is observed over a wide range supports theoretical predictions that the region of the profile nearest the surface is independent of molecular weight and that only the tail of the distribution varies with molecular weight. The variation with bulk concentration indicates a thin polymer-rich layer (~90 ± 10%) near the surface which decays to under 20% within the first ~20 Å. These results are consistent with recent neutron reflectivity data reported for PDMS at the air–toluene interface.[5] In the near-Θ solvent BC, the profile decays from the surface much more slowly than in BH. We conclude that the profile is not consistent with a step function (assuming $\phi_s > 0.8$) but is well described by both scaling and mean-field profiles. The adsorbed amount is roughly 4 times greater than in the good solvent BH, which is consistent with previous ellipsometric data at a solid–liquid interface. In addition, there appears to be a higher dependence on molecular weight for the region near the surface than in the good solvent. Finally, we observe a qualitative change in the profile in the proximity of the coexistence curve ($T < T_c$), where the results cannot be described by the Θ-solvent predictions of scaling or mean-field theories or by single step profiles.

Acknowledgment. We have benefited from discussions with Phil Pincus, David Andelman, and Scott Barton. We also thank Robert Cortes for technical assistance with the fluorescence experiments. We thank Hubert Hervet at the College de France for the use of the light scattering spectrometer for the measurement of the critical temperature for the 140K sample. M.S.K. was supported by Postdoctoral Fellowships from Elf Aquitaine (Direction de la Recherche du Developpement et de l'Innovation) and CNRS.

References and Notes

(1) Cohen Stuart, M. A.; Cosgrove, T.; Vincent, B. *Adv. Colloid Interface. Sci.* **1986**, *24*, 143.
(2) Patel, S.; Tirrell, M. *Annu. Rev. Phys. Chem.* **1989**, *40*, 597.
(3) Cosgrove, T. *J. Chem. Soc., Faraday Trans.* **1990**, *86*, 1323.
(4) Lee, L. T.; Guiselin, O.; Farnoux, B.; Lapp, A. *Macromolecules* **1991**, *24*, 2518.
(5) Guiselin, O.; Lee, L. T.; Farnoux, B.; Lapp, A. *J. Chem. Phys.* **1991**, *95* (6), 4632.
(6) Barton, S. W.; Bosio, L.; Cortes, R.; Rondelez, F. *Europhys. Lett.* **1992**, *17* (5), 401.
(7) Jones, I. S.; Richmond, P. *J. Chem. Soc., Faraday Trans. 2* **1977**, *73*, 1062.
(8) Scheutjens, J. M. H. M.; Fleer, G. J. *J. Phys. Chem.* **1979**, *83*, 1619.
(9) de Gennes, P.-G. *Macromolecules* **1981**, *14*, 1637.
(10) Cosgrove, T.; Heath, T. G.; Ryan, K.; Crowley, T. L. *Macromolecules* **1987**, *20*, 2879.
(11) Auvray, L.; Cotton, J. P. *Macromolecules* **1987**, *20*, 202.
(12) di Meglio, L. M.; Ober, R.; Paz, L.; Taupin, C.; Pincus, P. *J. Phys. (Paris)* **1983**, *44*, 1035.
(13) Ober, R.; Paz, L.; Taupin, C.; Pincus, P.; Boileau, S. *Macromolecules* **1983**, *16*, 50.
(14) Bloch, J. M.; Sansone, M.; Rondelez, F.; Peiffer, D. G.; Pincus, P.; Kim, M. W.; Eisenberger, P. M. *Phys. Rev. Lett.* **1985**, *54*, 1039.
(15) Yun, W. B.; Bloch, J. M. *J. Appl. Phys.* **1990**, *68*, 1421.
(16) Brunel, M. *Acta Crystallogr.* **1986**, *A42*, 304.
(17) Parratt, L. G. *Phys. Rev.* **1954**, *95*, 359.
(18) Kawaguchi, M.; Takahashi, A. *Macromolecules* **1983**, *16*, 1465.
(19) Caucheteux, I.; Hervet, H.; Jerome, R.; Rondelez, F. *J. Chem. Soc., Faraday Trans.* **1990**, *86*, (9), 1369.
(20) Bouchaud, E.; Daoud, M. *J. Phys. (Paris)* **1987**, *48*, 1991.
(21) We again point out that our conclusions are based on the data for $\theta < 1$ mrad, where the penetration depth is ~40 Å and the largest variation is observed with ϕ_b.
(22) Richmond, P.; Lal, M. *Chem. Phys. Lett.* **1974**, *24*, 594.
(23) Ingersent, K.; Klein, J.; Pincus, P. *Macromolecules* **1986**, *19*, 1374. Klein, J.; Pincus, P. *Macromolecules* **1982**, *15*, 1129.
(24) Johnson, H.; Granick, S. *Macromolecules* **1991**, *24*, 3023.
(25) In preparation.
(26) Lapp, A.; Herz, J.; Strazielle, C. *Makromol. Chem.* **1985**, *186*, 1919.
(27) Lapp, A.; Strazielle, C. *Makromol. Chem., Rapid Commun.* **1985**, *6*, 591.

Registry No. BH, 629-04-9; BC, 108-85-0.